Attitude Guidance and Control Law Design for the Science Phases of the SWARM-EX Mission

Athreya Gundamraj*, E. Glenn Lightsey†
Georgia Institute of Technology, Atlanta, GA, 30332, United States

The Space Weather Atmospheric Reconfigurable Multiscale Experiment (SWARM-EX) mission is a three 3U CubeSat mission which will collect plasma and atomic oxygen data in the upper atmosphere at unprecedented resolutions. The design and simulation of guidance laws and representative control algorithms for the major sub-modes within the science phases was conducted. While a baseline, radial-tangential-normal (RTN) tracking attitude profile meets the pointing requirements, poor solar energy absorption and downlink throughput resulted in a need for optimal attitude states which utilize the available margins on each requirement. A numerical optimization framework was developed which computes the optimal attitude by solving a constrained minimization problem. The results demonstrate a significant improvement when the pointing requirement margins are considered. To develop a flight software implementation, a constrained guidance law was devised which computes a commanded direction for one body frame vector such that a secondary body vector is maximizing alignment. The constrained guidance solution was integrated with the XACT-15 commanding architecture to create pseudocode for the complete ADC guidance software. Simulations in STK verified the ability of the ADC guidance software to output commands which satisfy the pointing requirements, and a reaction wheel controller was simulated to model spacecraft slews as the guidance software outputs commands. A representative desaturation controller was developed which enables near-complete wheel desaturation within one orbit period. These analyses resulted in a robust set of analysis tools and models that not only characterize the performance of the ADC system, but also will continue to mature as the spacecraft and mission design progress.

I. Introduction

A. Mission Overview

The Space Weather Atmospheric Reconfigurable Multiscale Experiment (SWARM-EX) mission is a three 3U cube satellite (CubeSat) science mission intended to study magnetic anomalies in Earth's upper atmosphere. By utilizing novel techniques in spacecraft formation-flying, inter-satellite communication, and CubeSat propulsion, the CubeSats will gather plasma and atomic oxygen data at unprecedented spatial and temporal resolutions [1]. The science goal is to understand key features of the equatorial thermal anomaly (ETA) and equatorial ionization anomaly (EIA): highly-varying temperature and electron density variations at low magnetic latitudes [2]. Initially conceived in the National Science Foundation (NSF) CubeSat Innovations Ideas Lab workshop in 2019, the SWARM-EX mission is comprised of six universities, over 25 students, and an array of subject matter experts actively working on the project. The mission completed its preliminary design review in February 2020 and is pursuing a launch date in 2024 with a preferred method of ISS deployment.

The three CubeSats are all built identically and will be flying in an highly autonomous formation. Each spacecraft hosts orbit guidance, navigation, and control (OGNC) software to plan formation keeping and reconfiguration maneuvers [3,4]. The maneuvers are transmitted as commands and a 3D-printed, cold-gas propulsion unit that provides the corresponding impulses [5]. A UHF frequency link between the three spacecraft serves enables autonomous collision avoidance, and each spacecraft is equipped with an X-band radio for ground communication. As depicted in Fig. 1, the mission consists of science (SCI) and OGNC phases which aim to meet different sets of mission objectives. The formation will spend approximately 75% of the nominal mission in the science phases, the more challenging phases

*Graduate Student, Georgia Tech Space Systems Design Lab
†Faculty Advisor, Georgia Tech Space Systems Design Lab

from an attitude determination and control (ADC) perspective. Thus, this paper details the ADC system design and analysis of each SWARM-EX CubeSat when in the science phases.

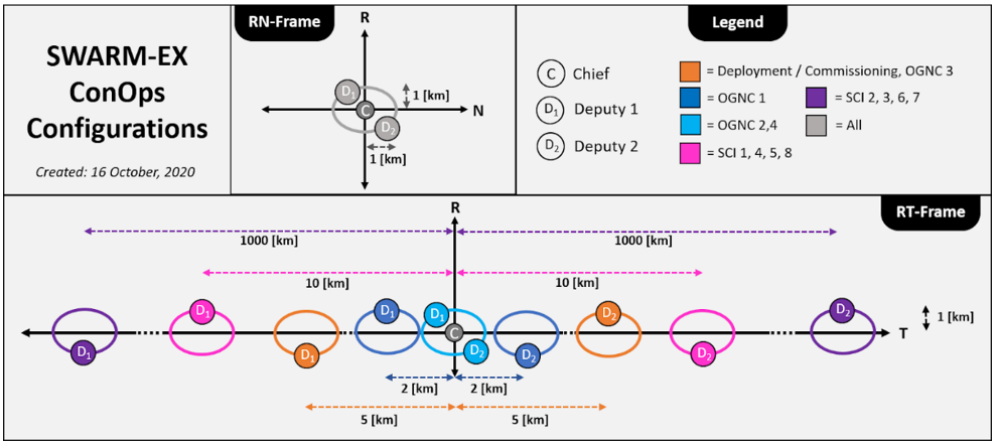

Fig. 1 mission phases defined in the SWARM-EX concept of operations

B. Spacecraft ADC System Overview

Fig. 2 depicts the hardware layout of each CubeSat with the key pointing vectors defined in the spacecraft body frame. The Phi-Flux Experimental Probe (FIPEX) and Langmuir Probe (LP) are the onboard science instruments and are fixed in the same body frame direction. A single GNSS antenna patch is situated on the solar panel face. The propulsion system sits on the +Z side of the CubeSat and has a single nozzle pointing in the corresponding direction. a total of six pointing requirements exist throughout the mission; these requirements, along with their margins and rationale, are stated in Fig. 3.

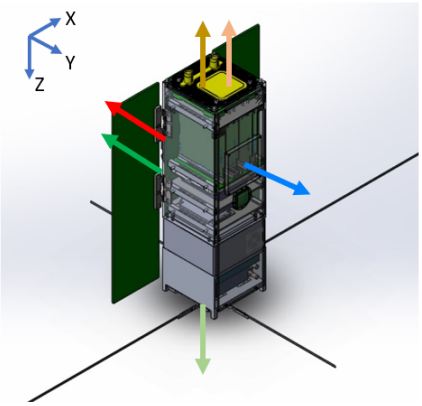

Vector Name	Body Frame Definition
Solar Panel Normal Vector	[0, -1, 0]
X-Band Antenna Vector	[0, 1, 0]
GNSS Antenna Vector	[0, -1, 0]
Propulsion Nozzle Vector	[0, 0, 1]
FIPEX Vector	[0, 0, -1]
Langmuir Probe Vector	[0, 0, -1]

Fig. 2 Spacecraft body frame and key pointing vector definitions

Each spacecraft will be equipped with an XACT-15: an ADC system supplied by Blue Canyon Technologies. The XACT-15 is equipped with two sun sensors placed on the spacecraft +Y and -Y faces, one star tracker, an inertial measurement unit, and two magnetometers for measurements. The XACT-15 also hosts three orthogonal torque rods and three orthogonal reaction wheels for actuation. On the spacecraft, the XACT-15 sits above the propulsion unit with the star tracker pointed in the +X direction. By selecting a system with a technology readiness level of 9, the mission risk is reduced and a highly capable unit is supplied to meet the challenging pointing needs of the mission.

Body Frame Vector	Pointing Direction	Margin	Rationale
Solar Panel Normal Vector	Sun	± 90°	For on-orbit power generation
X-Band Antenna Vector	Ground Station	± 18°	Pointing errors greater than the margin results in an ineffective gain
GNSS Antenna Vector	Zenith	± 30°	Ensures availability of GNSS data and similar GPS sat. coverage between spacecraft
Propulsion Nozzle Vector	Thrust Direction (provided by GNC)	± 0.5°	Stringent pointing prevents rapid accumulation of thrust errors
FIPEX Vector	Spacecraft velocity	± 30°	Science Data Collection
Langmuir Probe Vector	Spacecraft velocity	± 45°	Science Data Collection

Fig. 3 List of possible pointing requirements throughout the mission.

Within the science phases are four pointing sub-modes, and the table in Fig. 4 depicts each sub-mode with the pointing requirements it must satisfy. When in the data collection sub-mode, the spacecraft will collect measurements while maximizing power generation from its solar panels. Since the FIPEX will be shut down during eclipse periods for energy conversation, the FIPEX pointing requirement is only active in the sunlit region. When the spacecraft is within line of sight (LOS) of a ground station, the spacecraft will transfer to a downlink sub-mode. Depending on the whether the downlink period occurs in eclipse or in sunlight, the downlink sub-mode must satisfy either the FIPEX or LP pointing requirement. The GNSS antenna vector must be near-zenith pointed at least once per orbit for the OGNC software to re-establish its relative state. When maneuvering, the propulsion nozzle must be pointed in the desired direction (provided by the OGNC software) while the GNSS antenna gathers measurements for the OGNC software to accurately plan and execute a maneuver. Maneuvers will only occur before the mission shifts to the next science phase which is once every 30 days. Therefore, the CubeSat will be typically alternating between the data collection and downlink sub-modes when in the science phases of the mission and hence why these two sub-modes are the focus of the subsequent analyses. The safe mode is where the spacecraft remains sun-pointed as it resolves any anomalies before returning to normal operations.

Science Phase (SCI-1 through SCI-8)				
Pointing Constraint	Sub-Modes			
	Data Collection	Maneuvering	Downlink	Safe
Solar Panel Normal Vector	Maximize	Maximize		
X-Band Antenna Vector				
GNSS Antenna Vector	Once per Orbit		Once per Orbit	
Propulsion Nozzle Vector				
FIPEX Vector	If on Dayside		If on Dayside	
Langmuir Probe Vector			If on Nightside	

Not Required
Conditional
Required

Fig. 4 Pointing sub-modes in the science mission phases and their corresponding pointing requirements.

C. Feasibility Study

Before a quantitative analysis of the ADC system performance was conducted, a brief feasibility study was completed to confirm that the component placement depicted in Fig. 2 does not result in a null set of feasible attitude profiles. Fig. 5 depicts an attitude profile where the four pointing vectors in the various sub-modes of the science phases are simultaneously met. This baseline profile has the body frame tracking the radial (R), tangential (T), and normal (N) frame. In this profile, the X-band antennae can be pointed toward a ground station while the instrument and GNSS antenna requirements are satisfied. For formation reconfiguration maneuvers, the desired impulse will occur in either the tangential or anti-tangential direction. It is evident from Fig. 5 that GNSS antenna pointing is maintained while the propulsion nozzle is aligned with either of its possible directions. Thus, Fig. 5 serves as an existence proof that a set of attitude profiles exist which can meet the requirements for every sub-mode. However, preliminary data and

power budgets highlight that the RTN-tracking guidance law provides neither the solar energy absorption nor the data throughput required by the concept of operations. A more advanced attitude profile must be developed which utilizes the margins depicted in Fig. 3 to achieve sufficient power generation and downlink coverage.

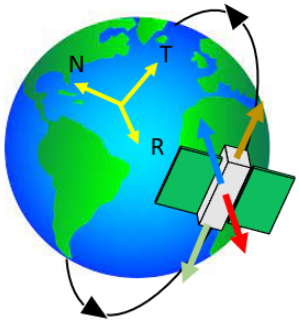

Vector Name	Body Frame Definition
GNSS Antenna Vector	[0, -1, 0]
X-Band Antenna Vector	[0, 1, 0]
FIPEX Vector	[0, 0, -1]
Propulsion Nozzle Vector	[0, 0, 1]

Fig. 5 Baseline attitude profile which demonstrates that all sub-mode pointing requirements can be met.

II. Attitude Guidance Laws

A. Numerical Optimization Approach

Utilizing the margins for each pointing requirement to maximize power generation and downlink data throughput will be formulated as inequality constraints that, along with an objective function, can be numerically solved. The objective function in this section will be for solar energy absorption, but an identical approach can be taken for data throughput. Several reference frames will be employed: the Earth-centered inertial (ECI, denoted in variables with I) frame, the RTN (R) frame, and the orbit (O) frame, also known as the perifocal frame. Shown in Fig. 6 are geometric representations of each frame for a case where right ascension of the ascending node (Ω) is 0. The orbit and ECI frames are fixed (for time scales on the order of an orbit period) as the RTN frame rotates about its z-axis along the orbit.

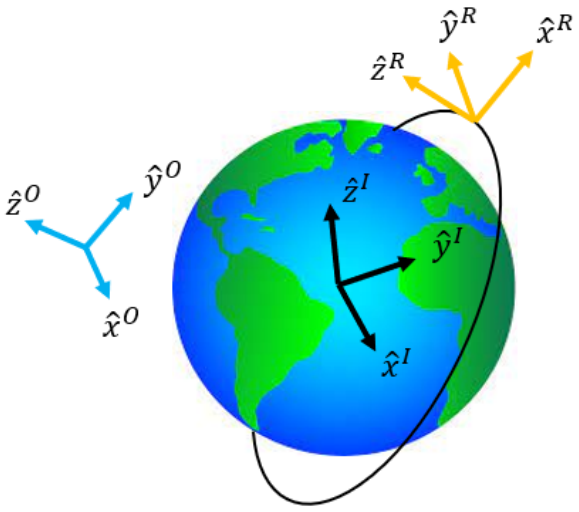

Fig. 6 Reference frame definitions for the numerical optimization problem.

By definition, the sun vector at the vernal equinox will point along the ECI x-axis. At other epochs, the sun vector can be described by a rotation ϵ (the obliquity of the ecliptic) about the ECI x-axis, and a subsequent rotation Γ (the ecliptic true solar longitude) about the new z-axis. Therefore applying the reverse sequence transforms the sun vector at vernal

equinox to that of any epoch:

$$\hat{s}^I = \begin{bmatrix} 1 & 0 & 0 \\ 0 & c(\epsilon) & -s(\epsilon) \\ 0 & s(\epsilon) & c(\epsilon) \end{bmatrix} \begin{bmatrix} c(\Gamma) & -s(\Gamma) & 0 \\ s(\Gamma) & c(\Gamma) & 0 \\ 0 & 0 & 1 \end{bmatrix} \begin{bmatrix} 1 \\ 0 \\ 0 \end{bmatrix} = \begin{bmatrix} c(\Gamma) \\ s(\Gamma)c(\epsilon) \\ s(\Gamma)s(\epsilon) \end{bmatrix} \tag{1}$$

$\epsilon \approx 23.45^o$ and Γ is a function of the epoch as it travels 360^o over a solar year: $\dot{\Gamma} = 360^o/365.25$ days. The transformation from the orbit frame to the ECI frame is a well known 3-1-3 transformation; without loss of generality, the argument of periapsis is set to 0 which gives:

$$D_O^I = \begin{bmatrix} c(\Omega) & -s(\Omega) & 0 \\ s(\Omega) & c(\Omega) & 0 \\ 0 & 0 & 1 \end{bmatrix} \begin{bmatrix} 1 & 0 & 0 \\ 0 & c(i) & -s(i) \\ 0 & s(i) & c(i) \end{bmatrix} = \begin{bmatrix} c(\Omega) & -s(\Omega)c(i) & s(\Omega)s(i) \\ s(\Omega) & c(\Omega)c(i) & -c(\Omega)s(i) \\ 0 & s(i) & c(i) \end{bmatrix} \tag{2}$$

Transforming the sun vector into the orbit frame obtains:

$$\hat{s}^O = \left(D_O^I\right)^T \hat{s}^I = \begin{bmatrix} s_1 \\ s_2 \\ s(\beta) \end{bmatrix} \triangleq \begin{bmatrix} c(\Omega)c(\Gamma) + s(\Omega)s(\Gamma)c(\epsilon) \\ -s(\Omega)c(i)c(\Gamma) + c(\Omega)c(i)s(\Gamma)c(\epsilon) + s(i)s(\Gamma)s(\epsilon) \\ s(\Omega)s(i)c(\Gamma) - c(\Omega)s(i)s(\Gamma)c(\epsilon) + c(i)s(\Gamma)s(\epsilon) \end{bmatrix} \tag{3}$$

Note that the third element is the sine of the β angle, and the s_1, s_2 definitions provide succinctness. The spacecraft attitude will be initialized with the profile defined in Fig. 5, which gives the following transformation:

$$D_O^B = \begin{bmatrix} 0 & 0 & 1 \\ -1 & 0 & 0 \\ 0 & -1 & 0 \end{bmatrix} \tag{4}$$

Adding in yaw, pitch, and roll degrees of freedom, which are the design variables in the optimization problem, in a 3-2-1 scheme obtains:

$$\begin{aligned} D_O^B &= D_x(\phi)D_y(\theta)D_z(\psi) \begin{bmatrix} 0 & 0 & 1 \\ -1 & 0 & 0 \\ 0 & -1 & 0 \end{bmatrix} \\ &= \begin{bmatrix} -s(\psi)c(\theta) & s(\theta) & c(\psi)c(\theta) \\ -c(\phi)c(\psi) - s(\phi)s(\psi)s(\theta) & -c(\theta)s(\phi) & c(\psi)s(\phi)s(\theta) - c(\phi)s(\psi) \\ c(\psi)s(\phi) - c(\phi)s(\psi)s(\theta) & -c(\phi)c(\theta) & s(\phi)s(\psi) + c(\phi)c(\psi)s(\theta) \end{bmatrix} \end{aligned} \tag{5}$$

Taking the transpose and applying it to the solar panel normal vector ($\vec{P}$) and FIPEX vector ($\vec{F}$) obtains their representations in the orbit frame.

$$\vec{P}^O = \begin{bmatrix} c(\phi)c(\psi) + s(\phi)s(\psi)s(\theta) \\ c(\theta)s(\phi) \\ c(\phi)s(\psi) - c(\psi)s(\phi)s(\theta) \end{bmatrix}, \qquad \vec{F}^O = \begin{bmatrix} c(\phi)s(\psi)s(\theta) - c(\psi)s(\phi) \\ c(\phi)c(\theta) \\ -s(\phi)s(\psi) - c(\phi)c(\psi)s(\theta) \end{bmatrix} \tag{6}$$

The tangential direction rotates at the orbit rate n along the orbit z-axis, making it a time-varying vector in the orbit frame: $\hat{v}^O = [-s(nt),\ c(nt),\ 0]^T$, where t is the time from crossing the ascending node. Note that this assumes a perfectly circular orbit, which is acceptable considering the near-zero eccentricity of the ISS orbit. The angle between the velocity vector and the FIPEX vector must be within 30^o; using the dot product as a representation of angular separation creates an inequality constraint:

$$\vec{F}^O \cdot \hat{v}^O = [c(\psi)s(\phi) - c(\phi)s(\psi)s(\theta)]s(nt) + c(\phi)c(\theta)c(nt) \geq c(30^o) \tag{7}$$

As mentioned earlier, the goal is to maximize the angle between the solar panel normal vector and sun vector; taking the dot product of these two vectors creates the objective function:

$$\vec{P}^o \cdot \hat{s}^o = s_1[c(\phi)c(\psi) + s(\phi)s(\psi)s(\theta)] + s_2(\theta)s(\phi) + s(\beta)[c(\phi)s(\psi) - c(\psi)s(\phi)s(\theta)] \tag{8}$$

Compiling Eqns. (7)-(8) into a canonical optimization problem formulation obtains:

$$\begin{aligned} \min_{\phi,\theta,\psi} \quad & -s_1[c(\phi)c(\psi) + s(\phi)s(\psi)s(\theta)] - s_2(\theta)s(\phi) + s(\beta)[c(\psi)s(\phi)s(\theta) - c(\phi)s(\psi)] \\ s.t. \quad & [c(\phi)s(\psi)s(\theta) - c(\psi)s(\phi)]s(nt) - c(\phi)c(\theta)c(nt) + c(30^o) \leq 0 \end{aligned} \tag{9}$$

This methodology is robust to additional constraints and varying objective functions as it simply requires adjusting, or adding, dot products of vectors in the orbit frame. By implementing the *fmincon()* function in *MATLAB()*, the solution to the optimization problem in Eqn. (9) was numerically computed over a period of the orbit. Using ISS parameters, the altitude and inclination were defined to be 410 km and 51.6^o, respectively. For simplicity, a vernal equinox date was assumed: $\Gamma = 0$. Two right ascension of the ascending node values were tested to validate the optimal solution, as shown in Fig. 7.

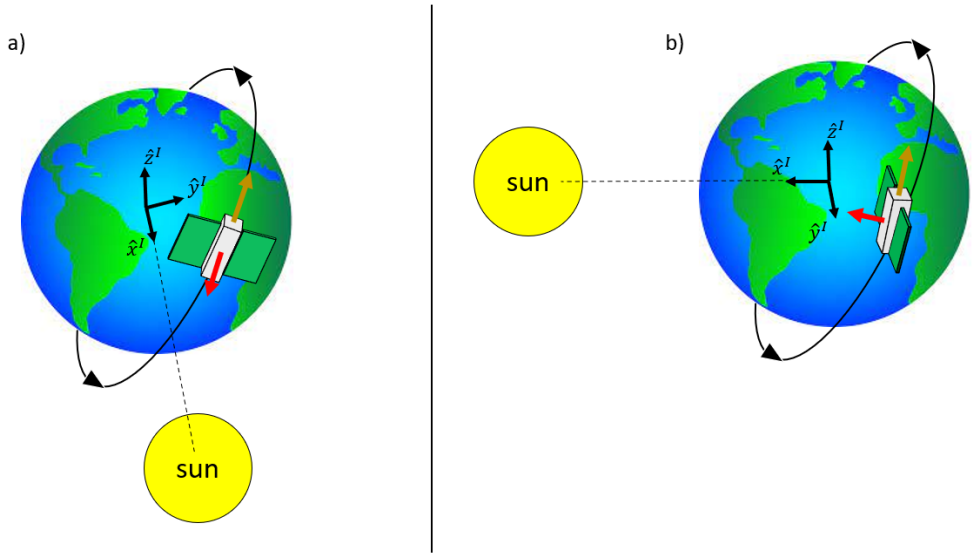

Fig. 7 Test cases for the numerical optimization solver: a) $\Omega = 0^o$, b) $\Omega = 90^o$.

Fig. 8 depicts the optimal Euler angles, the solar panel-sun angle, and instrument-zenith angle for a case where $\Omega = 0^o$. Since the sun is along the vernal equinox direction, the instrument pointing requirement is initially inactive and the solar panels face the sun directly. The spacecraft remains in an inertially fixed attitude profile until the instrument pointing constraint is active; from this instance forward, the spacecraft tracks the RTN frame until the constraint becomes inactive again when the spacecraft is approaching the ascending node. Since generated power is directly proportional to the cosine of the solar panel-sun angle, numerically integrating the solar panel-sun angle is a comparable metric to compare the performance of different attitude profiles. As shown in Fig. 10, the optimal attitude profile resulted in a 52% increase in generated power.

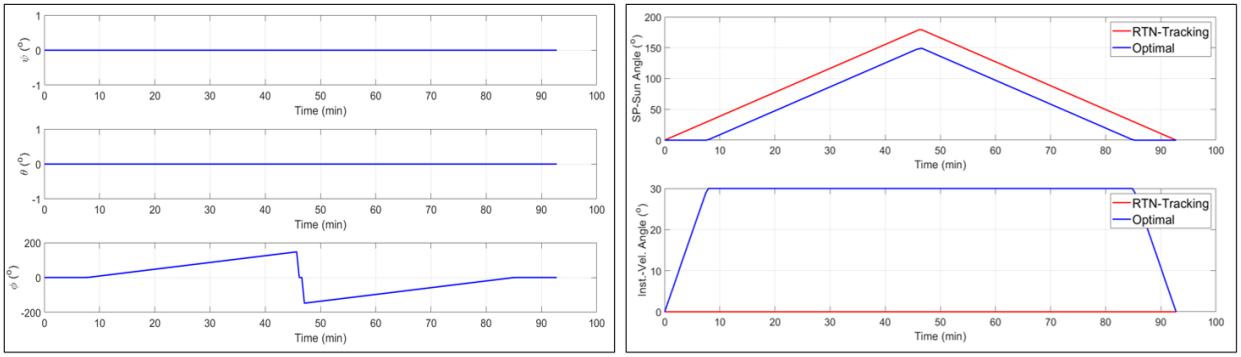

Fig. 8 Optimal Euler angles and resulting profile angles for the $\Omega = 0^o$ case.

Fig. 9 depicts the results when $\Omega = 90^o$. The initial yaw and roll angles rotate the solar panels towards the sun but the active instrument pointing constraint prevents perfect alignment with the sun vector. This perfect alignment does occur at true anomalies of 90^o and 270^o. The discontinuities in pitch angle (θ) at approximately 47 minutes is due to angle domain restrictions and thus is not a physically real rotation. The discontinuities at approximately 24 and 68 minutes will require the spacecraft to slew; Section III.A discusses the implications of these re-orienting slews on the attitude controller. The second row in Fig. 10 highlights that the optimal profile results in a remarkable 5.04x increase in generated power. This is due to the RTN-tracking profile causing the solar panel-sun angle to be greater than 90^o, which results in no solar energy absorption, for a majority of the orbit.

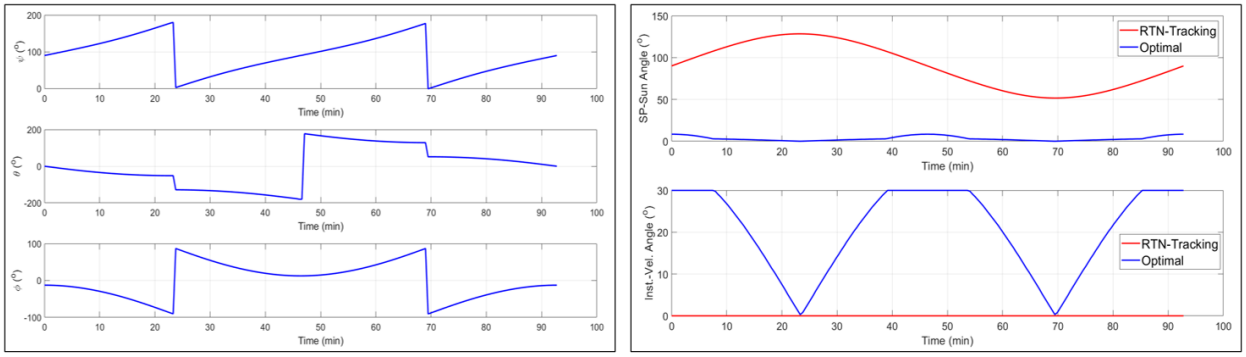

Fig. 9 Optimal Euler angles and resulting profile angles for the $\Omega = 90^o$ case.

Longitude of the Ascending Node (°)	Generated Power (units)	
	RTN-Tracking	Optimal
0	1771.70	2699.28
90	1100.46	5551.73

Fig. 10 Units of power generated for the various test cases and attitude profiles.

The results in Fig. 10 highlight that optimal attitude profiles result in significant improvement for generating power via solar panels when compared to the baseline, RTN-tracking profile. However, it is difficult, and outside the scope of the SWARM-EX mission, to implement an onboard numerical optimizer for attitude guidance. This analysis serves as a proof-of-concept that power generation can be significantly improved and results in a robust tool for numerical attitude optimization, and a separate approach must be considered to implement on-orbit optimal profiles.

B. Constrained Guidance Law

Fig. 4 highlights that a majority of the pointing profiles involve constraining a body frame vector within a cone of margin while maximizing alignment of a second, orthogonal body frame vector with an external reference. A constrained guidance law is devised which utilizes relative vector geometries to compute the commanded direction of the constrained body frame vector such that the second body frame vector alignment is optimized. This derivation is adapted from an analysis completed by D. Fitzpatrick of the SWARM-EX Team [5]. The constrained body frame vector and second body frame vector are denoted as $\hat{b}_1$ and $\hat{b}_2$, respectively, with $\hat{b}_1$ and $\hat{b}_2$ being orthogonal to each other. $\hat{b}_1$ is constrained such that its angle α with external reference vector $\vec{r}_1$ shall be no greater than α_{max}, and the guidance law will compute the commanded direction of $\hat{b}_1$ which minimizes angular separation between $\hat{b}_2$ and a second external reference vector $\hat{r}_2$. Without loss of generality, all vectors will be unit vectors.

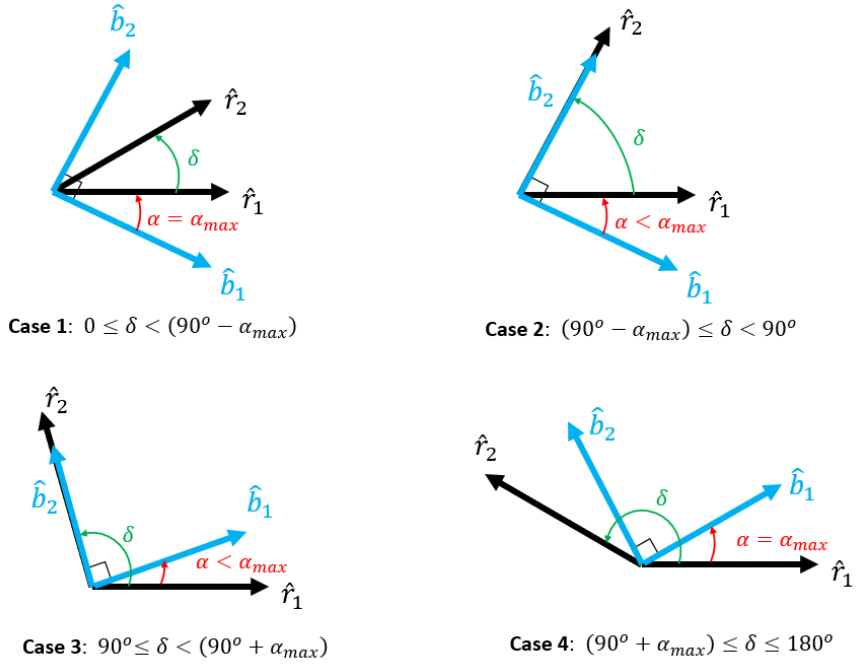

Fig. 11 Different cases for the development of the constrained guidance law.

Let δ be the angle between $\hat{r}_1$ and $\hat{r}_2$. As shown in Fig. 11, four cases are derived based on δ. In Case 1, δ is sufficiently small to activate the $\hat{b}_1$ pointing constraint and prevent optimal alignment of $\hat{b}_2$ with $\hat{r}_2$. Case 4 is a similar result but with δ being sufficiently large to prevent $\hat{b}_2$ alignment. In Cases 2 and 3, $\delta \in (90^o - \alpha_{max}, 90^o + \alpha_{max})$ which enables perfect $\hat{b}_2$ alignment. Utilizing vector geometries, the commanded direction of $\hat{b}_1$ can be expressed as a linear combination of $\hat{r}_1$ and $\hat{r}_2$ [6]:

$$\hat{b}_1 = \begin{cases} \hat{r}_1 - \left[\frac{sin(\alpha_{max})}{\sin(180^o - \alpha_{max} - \delta)}\right]\hat{r}_2 & 0^o \leq \delta < 90^o - \alpha_{max} \\ \hat{r}_1 - [\sin(90^o - \delta)]\hat{r}_2 & 90^o - \alpha_{max} \leq \delta < 90^o \\ \hat{r}_1 - [\sin(\delta - 90^o)]\hat{r}_2 & 90^o \leq \delta < 90^o + \alpha_{max} \\ \hat{r}_1 - \left[\frac{\sin(\alpha_{max})}{\sin(\delta - \alpha_{max})}\right]\hat{r}_2 & 90^o + \alpha_{max} \leq \delta < 180^o \end{cases} \tag{10}$$

To summarize, Eqn. (10) is a guidance law which computes the direction to point $\hat{b}_1$ such that the alignment of $\hat{b}_2$ with $\hat{r}_2$ is maximized. From a flight software perspective, the guidance law can be written as:

$$\hat{b}_1 = constrained\_guidance(\hat{r}_1,\ \hat{r}_2,\ \alpha_{max}) \tag{11}$$

Vectors $\hat{r}_1$ and $\hat{r}_2$ must be external vectors that the navigation software can provide estimates of, and α_{max} can be a tabulated list, similar to what is shown in the third column of Fig. 3.

C. Integration with XACT-15

In the fine reference mode of the XACT-15, one method for attitude commanding is to supply 4 vectors: a primary body frame vector ($\hat{b}_p$), a secondary body frame vector ($\hat{b}_s$), a primary external vector ($\hat{r}_p$), and a secondary external vector ($\hat{r}_s$). The XACT-15 will point $\hat{b}_p$ towards $\hat{r}_p$ and while holding this equality constraint, then maximize the alignment between $\hat{b}_s$ and $\hat{r}_s$. This equality constraint of the XACT-15 is why the constrained guidance law in Section II.B is required: the constrained guidance law accepts an inequality constraint with α_{max} margin and outputs an external direction (optimized for $\hat{b}_2$ alignment) that can be transmitted as an input to the XACT-15 software. The pseudocode function call to represent the XACT-15 software in this paper is a void method: *adc_sw*($\hat{b}_p$, $\hat{b}_s$, $\hat{r}_p$, $\hat{r}_s$). To define the complete SWARM-EX ADC guidance law, the following vectors in Fig. 12 are defined.

Sun vector	$\hat{s}$	Velocity vector	$\hat{v}$
Ground Station Vector	$\hat{g}$	Solar Panel Normal vector	$\hat{P}$
Instrument vector	$\hat{F}$	X-Band Antenna vector	$\hat{X}$
GNSS Antenna vector	$\hat{G}$		

Fig. 12 Vector definitions for ADC guidance software pseudocode.

Pseudocode for the SWARM-EX ADC guidance software when in the science phases is shown in Fig. 13. The inputs are vector estimates from the navigation software. The ADC software can track and measure eclipse periods using onboard ephemerides and sun sensors. Ground station LOS determination will either be from ground-commanded downlink time periods or onboard LOS calculations discussed in Section III.A.

Algorithm 1: SWARM-EX ADC Guidance Software

Input: $\hat{v}, \hat{g}, \hat{z}$ (from navigation software)

```
if in_eclipse then
    if in_los then
        r̂_p = constrained_guidance(v̂,ĝ,45°)
        adc_sw(F̂,X̂,r̂_p,ĝ)
    else
        adc_sw(F̂,X̂,v̂,ẑ)
    end
else
    if in_los then
        r̂_p = constrained_guidance(v̂,ĝ,30°)
        adc_sw(F̂,X̂,r̂_p,ĝ)
    else
        r̂_p = constrained_guidance(v̂,ŝ,30°)
        adc_sw(F̂,P̂,r̂_p,ŝ)
    end
end
```

Fig. 13 Pseudocode for SWARM-EX ADC guidance software.

If the CubeSat is in eclipse and within LOS of a ground station, then the constrained guidance law will provide a commanded direction for instrument pointing which maximizes X-Band antenna alignment towards the station. If there is no downlink opportunity when in eclipse, the CubeSat implements a RTN-tracking profile with the instruments and GNSS antenna in the velocity and zenith direction, respectively. If the CubeSat is in sunlight and within LOS of a ground station, the constrained guidance law is provided a lower α_{max} of 30^o when compared to in eclipse since the FIPEX vector has a lower pointing margin than the LP (see Fig. 4). When not communicating with a ground station, the CubeSat will employ the constrained guidance law to determine instrument pointing which maximizes power generation. Verification of this guidance law is discussed in the subsequent section.

III. Attitude Control Laws

A. Reaction Wheel Controller

To simulate the SWARM-EX guidance software and obtain the spacecraft attitude states, the Software Tool Kit (STK) simulation platform was implemented. Using custom-defined Visual Basic scripts and the STK attitude profiler, the constrained guidance law and XACT-15 software were simulated. Shown below are the orbital elements employed for each simulation. The selected epoch is vernal equinox of 2024, which, along with the selected orbit parameters, represent an ISS orbit with a near-zero beta angle: the beta angle at which the most number of slews occur due to the consistent eclipse periods.

$$a = 6800\ km, \quad e = 0.0002598, \quad i = 51.64^o, \quad \omega = 262.442^o, \quad \Omega = 15^o \tag{12}$$

For LOS determination, the spacecraft "up" coordinate in an East-North-Up topocentric frame was computed from its LASP-relative position vector in the Earth-Centered-Earth-Fixed frame.

$$\begin{aligned} U &= \cos(\lambda_{gs})\cos(\phi_{gs})x_F + \sin(\lambda_{gs})\cos(\phi_{gs})y_F + \sin(\phi_{gs})z_F \\ el &= \sin^{-1}\left[\frac{U}{\sqrt{x_F^2 + y_F^2 + z_F^2}}\right] \end{aligned} \tag{13}$$

In Eqn. (13), ϕ_{gs} and λ_{gs} are the latitude and longitude of the LASP station, respectively. If the spacecraft elevation is greater than the minimum elevation of 5^o, then it is assumed that downlink will occur.

The STK software assumes perfect control: the spacecraft instantaneously updates its attitude based off the ADC software output. Thus, the time history of the attitude quaternions from STK was exported to serve as a time-tagged list of the attitude states the attitude controller must orient the spacecraft to. For precise pointing, the XACT-15 utilizes three orthogonal reaction wheels with a saturation limit of 15 mN*m*s per wheel. For this analysis, the reaction wheel frame, body frame, and principal frame are assumed to all be aligned. The inertia of the spacecraft was computed by assuming a uniform density 3U CubeSat with extended solar panels on the -Y face. The table in Fig. 14 shows the dimensions implemented for the body and CubeSat to obtain an inertia tensor of: $I = diag([0.1312,\ 0.14,\ 0.1102])$.

Body Mass [kg]	3.6	Body Dimensions [cm]	30 x 10 x 10
Solar Panel Mass [kg]	0.4	Solar Panel Dimensions [cm]	30 x 30 x 0.05

Fig. 14 Simplified spacecraft mass and dimension values for inertia estimation.

To model the XACT-15 reaction wheel controller, an attitude regulator law is designed. The error between the current state (q) and the commanded state (q_c) is defined as an error quaternion:

$$\delta q = q \otimes q_c^{-1} \tag{14}$$

Using the components of the error quaternion, a feedback torque provided by the reaction wheels ($\vec{L}_c$) is computed via a proportional derivative control law [7]:

$$\vec{L}_c = -k_p\ sign(\delta q_4)\ \vec{\delta q}_{1:3} - k_d\vec{\omega} \tag{15}$$

The terms $\vec{\delta q}_{1:3}$ and δq_4 and the vector and scalar components of the error quaternion, respectively. The stability of the controller in Eqn. (15) is proven via Lyapunov's direct method [7]. The *sign(δq_4)* term in Eqn. (15) ensures that the controller provides the shortest path to the commanded attitude. It is assumed that the spacecraft is a rigid body adhering to Euler's equations for rotational dynamics, and due to Newton's Third Law, the reaction wheels will exhibit a negative torque than what is administered on the CubeSat. Eqn. (16) depicts the equations of motion used to simulate the spacecraft attitude dynamics with the feedback controller. It is assumed that the only torques acting on the spacecraft are that of the reaction wheels.

$$\begin{aligned} \dot{q} &= \frac{1}{2}q \otimes \vec{\omega} \\ I\dot{\vec{\omega}} &= -\vec{\omega} \times (J\vec{\omega}) + \vec{L}_c \\ \dot{\vec{h}} &= -\vec{\omega} \times \vec{h} - \vec{L}_c \end{aligned} \tag{16}$$

The dynamics were propagated using a Runge-Kutta 4 integrator in MATLAB, and perfect navigation was assumed. The CubeSat was specified with an initial attitude defined per the ADC guidance software in Fig. 13, zero angular rate, and initial wheel momentum of 0.5 mN*m*s along each axis. Preliminary simulations were employed to tune the gains to: $k_p = 0.01$, $k_d = 0.05$. For a step input, these gains resulted in an overdamped response where the commanded torques did not saturate the wheels but provided sufficient actuation to ensure settling times of approximately 30s.

Shown in Fig. 15-17 are plots of the spacecraft angular rates, reaction wheel momentum, and angles over two orbital periods. The gray and yellow shading represent the eclipse and sunlit portions of the orbit, respectively. The red rectangles are regions in which the spacecraft is in LOS of the LASP ground station. The behavior in these plots directly match the expected performance based off the flight software pseudocode in Fig. 13. When entering eclipse periods, the CubeSat performs a slew to follow a RTN-tracking attitude profile; this is evident at approximately 55 minutes as the instrument-velocity angle and GNSS antenna-zenith angles both settle to 0^o shortly after. When entering the sunlit region, the spacecraft slews its solar panels toward the sun and the instrument-velocity angle instantly reaches its maximum allowable value of 30^o to increase solar energy absorption. In both downlink periods the X-Band-ground station angle reaches 0^o, entailing that the spacecraft slews to align its X-Band antenna with the ground station vector. The first plot in Fig. 17 depicts that the instrument requirement is never violated, which is expected when in the data collection and downlink sub-modes.

The reaction wheel angular momentum peaks to as high as 9 mN*m*s each slew, and the spacecraft experiences angular rates up to approximately 7 deg/s which will likely disrupt star tracker estimation. In this case, the navigation software runs off the IMU until the star tracker stabilizes, which requires up to 5 minutes. Star tracker fixes are only required when GNSS measurements are collected to update the OGNC states and per Fig. 4, this is conducted once per orbit. Therefore, as long as one instance exists along the orbit where the star tracker provides estimates when a GNSS measurement is collected, the OGNC software requirement is satisfied. The long eclipse periods ensure this will occur but if an issue is apparent at a later date, the controller gains can be adjusted to reduce the peak angular rates; the only consequence being a larger settling time. Fig. 15-17 not only verifies the ability of the ADC guidance software to command optimal attitude profiles given the constraints of each pointing vector, but also demonstrates the ability of a PD reaction wheel controller, a controller similar to what the vendor will program into the XACT-15 units, to achieve the desired pointing.

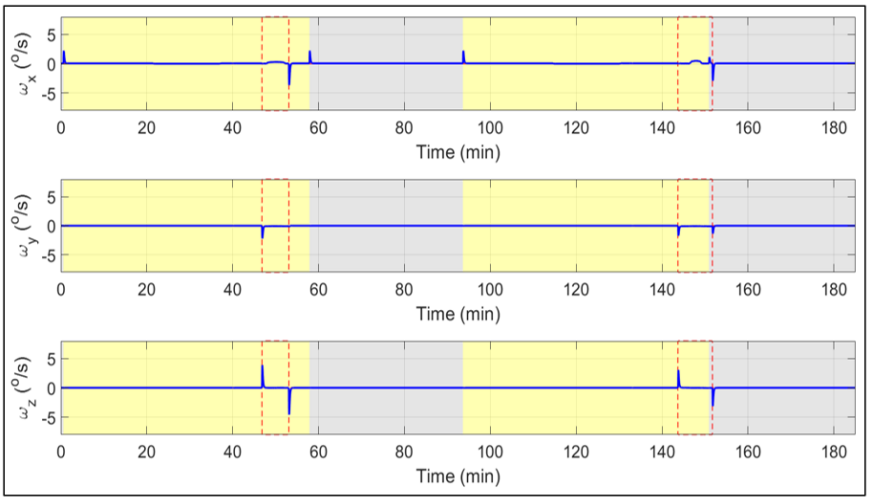

Fig. 15 Simulated spacecraft angular rates over two orbit periods when employing the ADC guidance software.

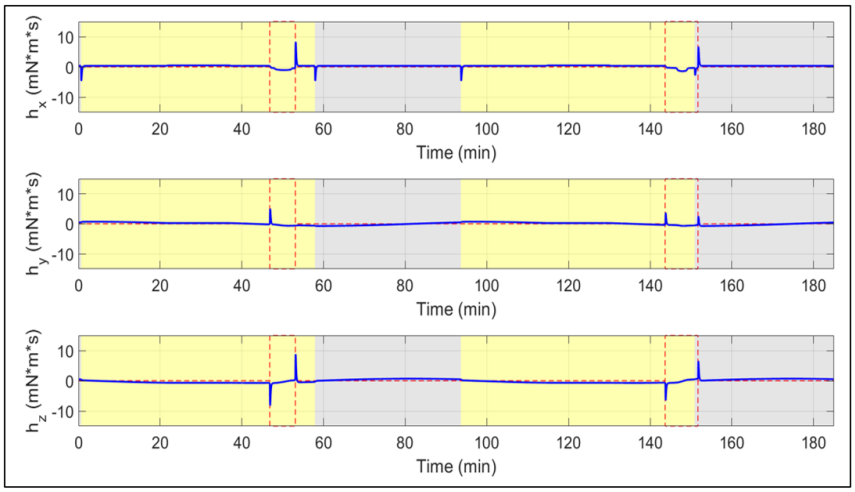

Fig. 16 Simulated reaction wheel angular momentum over two orbit periods when employing the ADC guidance software.

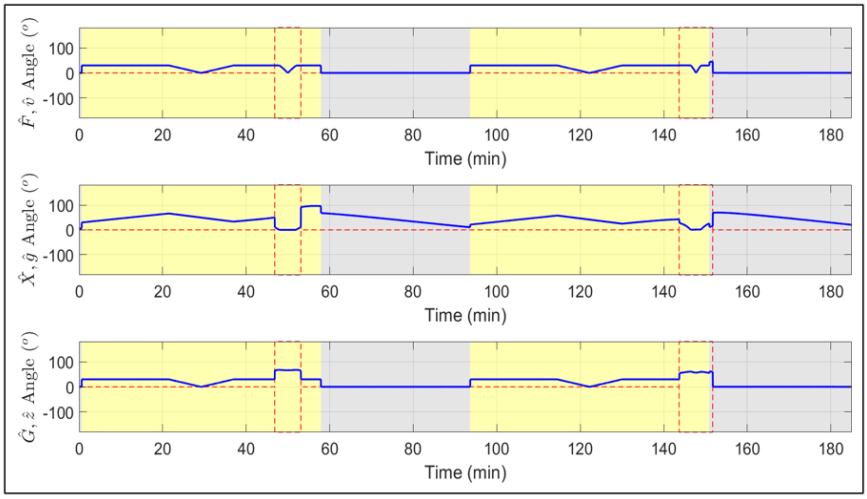

Fig. 17 Simulated spacecraft pointing angles over two orbit periods when employing the ADC guidance software.

B. Desaturation Controller

The presence of disturbace torques, frequent slewing of the CubeSat, and off-axis components from the propulsion system impulses may result in saturated reaction wheels. While the desaturation controller will be operating in the background throughout the sub-modes defined in Fig. 4, a sequence of large disturbace torques over a short period may still result in wheel saturation. This would cause the XACT-15 to enter a safe mode and prevent the CubeSat from conducting precise pointing until the wheels are desaturated. The propulsion system will not be utilized for momentum desaturation as the limited available propellant is solely allocated for formation-based maneuvers. Instead, the XACT-15 utilizes its three magnetic torque rods and magnetometer to desaturate the reaction wheels. The XACT-15 is delivered with a predefined desaturation function, so this design is intended to be representative of what the vendor will provide.

The desaturation controller will actuate the torque rods to create an internal magnetic moment which interacts with Earth's magnetic field to induce a torque on the spacecraft. For this analysis, it is assumed that the torque rods and reaction wheels are aligned with the spacecraft principal axes. Each torque rod in the XACT-15 has a maximum dipole moment (m_{max}) of 0.3 Am^2. At each update step, the magnetic moment to be induced in each torque rod will be

computed with the following control law:

$$\vec{m} = \frac{k}{||\vec{B}||}\vec{h} \times \hat{B} \tag{17}$$

k is the user-defined controller gain, $\vec{B}$ is the magnetic field vector in the spacecraft body frame (which will be measured via the onboard magnetometers), and $\vec{h}$ is the total angular momentum stored in the reaction wheels. If the magnetic moment computed from Eqn. (17) has a component along any axis greater than m_{max}, then that torque rod will be commanded to m_{max}. The dynamics can remain in the body frame, thus simplifying the angular momentum derivative to equal the induced magnetic torque:

$$\dot{\vec{h}} = \vec{m} \times \vec{B} \tag{18}$$

With a candidate Lyapunov function of $V = \frac{1}{2}\vec{h}^T I\vec{h}$, this controller is proven to be stable in practical applications [6].

The spacecraft mass and inertia properties defined in Section III.A were employed in the desaturation simulation. Each reaction wheel momentum was initially set to 90% of its saturation limit, which is likely when the XACT-15 would enter a safe mode to prioritize desaturation. The initial angular rate of the spacecraft is set to 0.5 deg/s, which is the "rotisserie" rate of the XACT-15 when in safe mode. The dynamics were propagated using a Runge-Kutta 4 integrator in *MATLAB*, and perfect navigation was assumed. The magnetic field model is generated via coefficients from the National Geophysical Data Center packaged into a *MATLAB* function [8]. Based on initial results, the controller gain was set to: $k = 0.0012$.

Fig. 18 depicts time histories of the reaction wheel angular momentum with the desaturation controller active. It requires approximately 90 minutes, or one orbit period, to desaturate the wheels to a near-zero angular momentum state. In practical applications, desaturation will occur until the wheels reach a non-zero minimum value set by the vendor. In Fig. 19, it is evident that as the reaction wheels slow down, the magnetic moments also approach zero which is expected since the desaturation algorithm is a proportional controller.

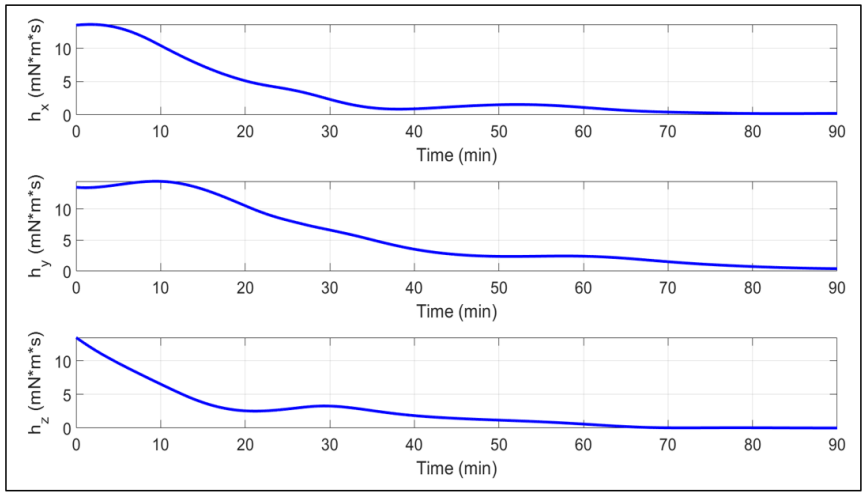

Fig. 18 Simulated reaction wheel angular momentum with an active desaturation controller.

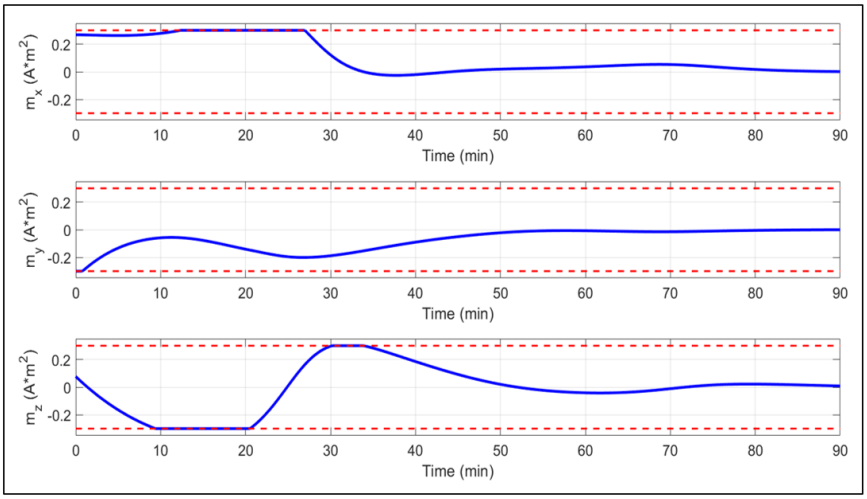

Fig. 19 Magnetic moments on each body frame torque rod during desaturation control.

IV. Conclusion

This paper began with a feasibility study demonstrating that an RTN-tracking attitude profile meets the pointing requirements in all science phase sub-modes defined in Fig. 4. The RTN-tracking attitude profile was established as a baseline, but poor solar energy absorption and downlink data throughput resulted in a need to study optimal attitude profiles which utilized the margins delineated in Fig. 3. By framing the optimal attitude as a solution to a constrained optimization problem, numerical results for several test cases were achieved which highlighted remarkable improvement in power generation: the $\Omega = 0^o$ and $\Omega = 90^o$ cases had 1.52x and 5.04x more solar energy absorbed with the optimal attitude profile. This proof of concept that optimal profiles lead to significant performance improvements resulted in the formulation of a constrained guidance law which determines the direction of body frame vector $\hat{b}_1$ such that the alignment between $\hat{b}_2$ and external vector $\hat{r}_2$ is maximized. The analytical solutions from this constrained guidance law allows for a straightforward implementation in flight software, and pseudocode in Fig. 13 was designed which integrates the guidance law with the XACT-15 commanding architecture. This ADC guidance software was simulated in STK, and a PD reaction wheel controller was tuned to simulate onboard actuation for slews. The guidance software was verified with a $\beta = 0^o$ test case, and the controller avoided wheel saturation while exhibiting settling times of approximately 30 s. A desaturation controller, representative of what the vendor will provide, was designed with utilizes torque rods to desaturate the reaction wheels. Preliminary simulation results show that reaction wheels at 90% momentum capacity can be reduced to near-zero angular momentum over one orbit period. An outcome of these analyses is a set of robust and representative tools to simulate and analyze the ADC system behavior in various mission phases.

V. Future Work

Moving forward, the next step is to model the ADC system behavior with simulated navigation software in the loop. This improvement would enable the simulations to better reflect the on-orbit performance of the CubeSats. Furthermore, external disturbance torques must be included in the attitude control models; these torques are non-negligible over extended periods of time and may result in activating the desaturation controller more often which increases the power draw of the XACT-15. The OGNC phase sub-modes are slightly less demanding than that of the science phases, so the tools and pseudocode in this paper can be readily adapted to analyze the OGNC phases of the mission. Lastly, the SWARM-EX systems and ADC teams must continue to work with Blue Canyon Technologies to ensure that all behaviors and functions of the XACT-15 are accounted for in the attitude profile design. Few examples of behaviors that are not currently simulated but must be examined are star tracker keep-out zones, dead bands for the desaturation controller, reaction wheel motor torque limits, and phenomenon which cause the XACT-15 to enter to its safe mode. With an upcoming critical design review followed by hardware delivery of the flight units, the ADC design for the SWARM-EX will continue to mature as it has implications on the concept of operations, system integration and test, and on-orbit performance, all of which impact mission success.

Acknowledgments

This material is based upon work supported by the National Science Foundation under Contract No. 1936537. Any opinions, findings, and conclusions or recommendations expressed in this material are those of the author(s) and do not necessarily reflect the views of the National Science Foundation. The author recognizes the SWARM-EX team for their continued support throughout the mission, and the cooperation of Blue Canyon Technologies during the procurement process of the XACT-15 units.

References

[1] Eberhart, M., Lohle, S., Steinbeck, A., Binder, T., Fasoulas, S., Measurement of atomic oxygen in the middle atmosphere using solid electrolyte sensors and catalytic probes, Atmospheric Measurement Techniques, 2015, Vol. 8, No.9, pp. 3701-3714, https://www.atmos-meas-tech.net/8/3701/2015/, doi: 10.5194/amt-8-3701-2015

[2] Appleton, E. V., "Two Anomalies in the Ionosphere", Nature, 157, 691–693, 1946.

[3] D'Amico S., Hunter R., Baker C., "Distributed Timing and Localization (DiGiTaL)" NASA Technical Reports Server 2017 https://ntrs.nasa.gov/search.jsp?R=20170011077

[4] D'Amico, S., "Autonomous Formation Flying in Low Earth Orbit," PhD Thesis, Delft University, 2010.

[5] Lightsey, E.G., Stevenson, T., and Sorgenfrei, M., "Development and Testing of a 3-D-Printed Cold Gas Thruster for an Interplanetary CubeSat." Proceedings of the IEEE, Vol. 106, No. 3, pp. 379-390, March 2018. doi: 10.1109/JPROC.2018.2799898

[6] Fitzpatrick, D., "SWARM-EX STK Concept of Operations Analysis Report", Unpublished Manuscript, University of Colorado Boulder, 2021.

[7] Markley, F. L., and Crassidis, J. L., "Fundamentals of Spacecraft Attitude Determination and Control", Vol. 33, Springer, 2014.

[8] Crassidis, J. L., and Junkins, J. L., "Optimal Estimation of Dynamic Systems", Chapman and Hall/CRC, 2011.